DOI: 10.13009/EUCASS2023-524
Aerospace Europe Conference 2023 – 10TH EUCASS – 9TH CEAS

Mid-Course Trajectory Optimization of VFDR Missiles via Pseudospectral Sequential Convex Programming

Boseok Kim, Chang-Hun Lee*†, Min-Jea Tahk*, Yongkun Lee**, Hong-Gye Sung***
** Aerospace Engineering, KAIST, ** Aerospace and Mechanical Engineering, Korea Aerospace University*
** 34141 Daejeon, Korea, ** 10540 Goyang, Korea*
kbobo6@kaist.ac.kr, lckdns@kaist.ac.kr, mjtahk@kaist.ac.kr, yongkun0116@kau.kr, hgsung@kau.ac.kr
† Corresponding Author

Abstract
This paper presents a mid-course trajectory optimization method for variable-flow ducted rocket (VFDR) missiles. The minimum-final time problem is defined by reflecting the dynamics and flight constraints. We represent the air mass flow rate as an analytic function of the state variables and construct an artificial neural network (ANN) for the thrust. The system equation is established by selecting the angle-of-attack and air-to-fuel ratio as control variables. Then, pseudospectral sequential convex programming (PSCP) is utilized to solve the problem. Numerical optimization results are provided to demonstrate the performance of the proposed method and examine the optimal trajectory pattern of the VFDR missiles.

1. Introduction

Compared to traditional air-to-air missiles (AAMs) equipped with a solid rocket engine, modern long-range AAMs adopt an air-breathing rocket engine with higher energy efficiency. It significantly increases the maximum effective range and interception capability of AMMs. Especially the variable-flow ducted rocket (VFDR) engine is known to be adequate for long-range AAMs as being utilized for the “Meteor” missiles, one of the most high-performance AAMs. In addition to the high energy efficiency, the VFDR engine can adjust the fuel mass flow rate by controlling the throttling valve. It provides the VFDR missiles an additional degree of freedom to steer them compared to solid rocket missiles that only can control the load factor. It allows the VFDR missiles to conduct more efficient energy management resulting in superior performance than the traditional ones.

The entire flight of medium or long-range missiles can be classified into three phases: the initial phase, mid-course phase, and terminal homing phase. The mid-course phase represents the flight interval from when the missile’s attitude is stabilized after the launch to the seeker’s lock-on moment. Since the mid-course phase occupies most of the flight time until reaching the target and determines the missile’s flight condition at the beginning of the homing phase, it greatly affects the interception performance of AAMs. Accordingly, mid-course guidance flight is typically conducted to maintain good conditions to intercept the target in the terminal phase. Hence, many studies have addressed the mid-course guidance problems as an optimal control problem, with the performance index of maximum-terminal velocity or minimum-final time [1]. Many studies were performed to solve the mid-course guidance problem for AAMs, especially for solid rocket missiles. In [2-6], the singular perturbation technique was utilized to obtain an approximate real-time solution by reducing the order of the problems. In [7-9], the neighboring optimal control theory was utilized to calculate the real-time correction for some pre-calculated nominal solutions. In [9], an analytic optimal mid-course guidance law was derived in terms of flight conditions, terminal constraints, and thrust effects. On the other hand, only a few studies exist to address the mid-course guidance for VFDR missiles. The singular perturbation technique was utilized for VFDR missiles in [10] to compute the lift and thrust commands for each flight phase, composed of ascent, cruise, and descent trajectories. In other works [11-12], the optimal mid-course guidance problems were converted into a parameter optimization problem and solved by applying a nonlinear programming (NLP) algorithm.

As seen above, many studies for solid rocket missiles applied optimal control theory to derive the approximate optimal guidance solution. However, for VFDR missiles, it is not easy to find that kind of work, and the existing one was limited to a particular flight situation. It comes from the fact that there exist an additional control variable and several flight constraints for VFDR missiles, which makes the problem more complicated. In addition, some inconsistent approximations made in the solution procedure may lead to losing the reliability and optimality of the solution for this constrained flight case. In such a case, the direct method, which discretizes the optimal control problem

DOI: 10.13009/EUCASS2023-524

and applies an appropriate solution algorithm, can be utilized to solve the problem [13], as done in the previous works [11-12]. It first discretizes the optimal control problem defined in the continuous-time domain to a parameter optimization problem and applies an adequate solution algorithm to solve the resulting optimization problem. The convergence properties of the solution then depend on certain factors, such as how the problem is formulated and which discretization method and solution algorithm are used.

Meanwhile, as it is known that the reusable launch vehicle "Falcon 9" utilized convex optimization for re-landing, many researchers have paid attention to using convex optimization for various aerospace engineering problems. However, many aerospace engineering problems accompany nonlinear dynamics with aerodynamic force and thrust, so it is quite restrictive to directly apply convex optimization to general aerospace engineering problems. As an alternative, sequential convex programming (SCP), an iterative convex optimization approach, has been studied to solve such non-convex problems in the convex optimization framework. SCP refers to the method that solves a non-convex optimization problem by solving a sequence of approximated convex optimization problems. Even though SCP generally does not ensure the deterministic convergence property and global optimality as for convex optimization, it has been successfully applied for various aerospace engineering problems such as landing guidance [14], missile guidance [15], and entry guidance [16] problems. These studies showed that SCP could provide a feasible solution within a reasonable computation time for a well-posed problem. At the same time, there have been some studies to improve the accuracy of SCP by combining it with a pseudospectral method called pseudospectral sequential convex programming (PSCP). The difference between the conventional SCP and PSCP is in the discretization manner. Conventional SCP utilizes uniform nodes and the trapezoidal rule for transcription. In contrast, PSCP employs pseudospectral methods that use a particular set of nonuniformly distributed nodes and global interpolation schemes with quadrature rules. This feature makes PSCP provide an accurate solution with a small number of nodes for a sufficiently smooth problem. PSCP has also been successfully applied for various aerospace engineering problems, as in [17-19].

Motivated by the above observations, this study establishes a mid-course trajectory optimization algorithm for VFDR missiles using PSCP. We first define a minimum-final time problem for the mid-course flight of VFDR missiles. Based on the air mass flow rate and thrust data, we represent the air mass flow rate as an analytic function of flight conditions and train an artificial neural network (ANN) for the thrust. This study proposes to choose the air-to-fuel ratio as a control variable instead of the fuel mass flow rate, which is the common choice for the VFDR missiles. This choice can reduce the number of nonlinear constraints in applying SCP and make the initialization process, providing the initial reference solution to start SCP, more straightforward owing to the regular solution pattern for the air-to-fuel ratio. Successive linearization is employed with a variable trust-region structure to compose an approximate convex optimization problem. In addition, an improved trust-region algorithm in [20] is applied to stabilize and accelerate the convergence of the solution.

The remainder of this paper is outlined as follows. In Section 2, the minimum-final time problem is formulated by introducing the dynamics and flight constraints for VFDR missiles and modeling the air mass flow rate and thrust using the pre-obtained data set. Section 3 elaborates on the PSCP algorithm to solve the defined minimum-final time problem. The system equation is first defined and discretized by applying the pseudospectral method. Then, SCP is utilized to solve the discretized problem. Section 4 provides numerical optimization results to demonstrate the proposed method's performance and investigate the optimal flight pattern of VFDR missiles. Finally, the conclusion of this study is given in Section 5.

2. Problem Formulation

2.1 Dynamics and flight constraints

This study considers the planar engagement in the vertical plane. In this circumstance, dynamics for VFDR missiles can be represented as:

$$\begin{aligned}
\dot{x} &= V\cos\gamma \\
\dot{h} &= V\sin\gamma \\
\dot{V} &= \frac{T\cos\alpha - D}{m} - g\sin\gamma \\
\dot{\gamma} &= \frac{T\sin\alpha + L}{mV} - \frac{g\cos\gamma}{V} \\
\dot{m} &= -\dot{m}_f
\end{aligned} \tag{1}$$

DOI: 10.13009/EUCASS2023-524

where x, h, V, γ, m denote the downrange, altitude, velocity, flight path angle, and mass, respectively. g denotes the constant gravity acceleration. L and D represent the aerodynamic lift and drag, which can be calculated by

$$\begin{aligned} L &= 0.5\rho V^2 S_{\text{ref}} C_L \\ D &= 0.5\rho V^2 S_{\text{ref}} C_D \end{aligned} \tag{2}$$

where S_{ref} means the reference area, and ρ denotes the air density. This study utilizes the exponential air density model and drag-polar for the aerodynamic coefficients as follows.

$$\begin{aligned} \rho &= \rho_0 e^{-h/h_s} \\ C_L &= C_{L,\alpha}\alpha \\ C_D &= C_{D,0} + KC_L^2 \end{aligned} \tag{3}$$

where ρ_0, h_s, $C_{L,\alpha}$, $C_{D,0}$, K are constant parameters to be determined according to the operating altitude range and missile configuration.

In Eq. (1), $\dot{m}_f$ means the fuel mass flow rate, and T represents the thrust generated by the VFDR engine. The thrust is determined by the mach number, altitude, angle-of-attack, and air-to-fuel ratio. The air-to-fuel ratio is defined by the ratio of fuel mass flow rate and air mass flow rate, which is again given as a function of the velocity, altitude, and angle-of-attack.

$$T = T\left(M, h, \alpha, AF\right) \tag{4}$$

$$AF = \frac{\dot{m}_a\left(V, h, \alpha\right)}{\dot{m}_f} \tag{5}$$

In this tsudy, the thrust and air mss flow rate data is contructed by following the literature [21-22]. For the steady operation of the VFDR engine, some flight constraints need to be satisfied. The available angle-of-attack range is limited for air-breathing, and the fuel mass flow rate is restricted to satisfy the pressure limit in the gas generator. In addition, the air-to-fuel ratio is constrained for stable combustion.

$$\alpha_{\min} \le \alpha \le \alpha_{\max} \tag{6}$$

$$AF_{\min} \le AF \le AF_{\max} \tag{7}$$

$$\dot{m}_{f,\min} \le \dot{m}_f \le \dot{m}_{f,\max} \tag{8}$$

2.2 Ducted rocket thrust modeling

This subsection constructs an analytic expression for the air mass flow rate and ANN for the thrust based on the pre-obtained data set to facilitate the trajectory optimization. The air mass flow rate is directly proportional to the velocity and air density, as it is well-known. Note that the dependency on the angle-of-attack differs according to the air intake design. This study models the angle-of-attack influence function by applying the polynomial curve-fitting on the data set. The curve-fitting result is depicted in Fig. 1. Denoting the polynomial influence function as $p(\alpha)$, the air mass flow rate can be represented as follows.

$$\dot{m}_a\left(V, h, \alpha\right) = \rho\left(h\right) \cdot V \cdot p\left(\alpha\right) \tag{9}$$

DOI: 10.13009/EUCASS2023-524

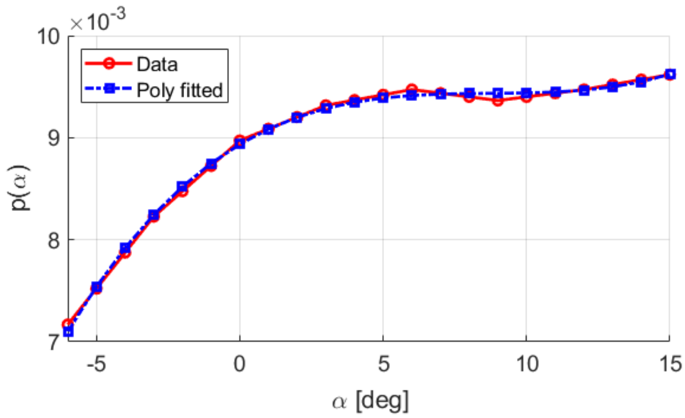

Figure 1: Angle-of-attack influence function for air mass flow rate

In contrast to the air mass flow rate, it is intractable to construct an analytical expression for the thrust due to its complicated nature, resulting from supersonic compression and combustion. Hence, this study utilizes an ANN, which can be regarded as a universal approximation function [23], to establish a smooth relation between the thrust and input variables. The depth of the hidden layer is set to 3, and each layer contains 15 nodes. The ANN is trained using 262,232 data sets consisting of flight conditions as the input layer and thrust as the output layer. The trained ANN for the thrust is denoted as follows.

$$T = T_{NN}\left(M, h, \alpha, AF\right) \quad \mathbf{(10)}$$

The training results for the thrust are given in Fig. 2. The trained ANN generally approximates the thrust data well, and the maximum error appears to be around 6%.

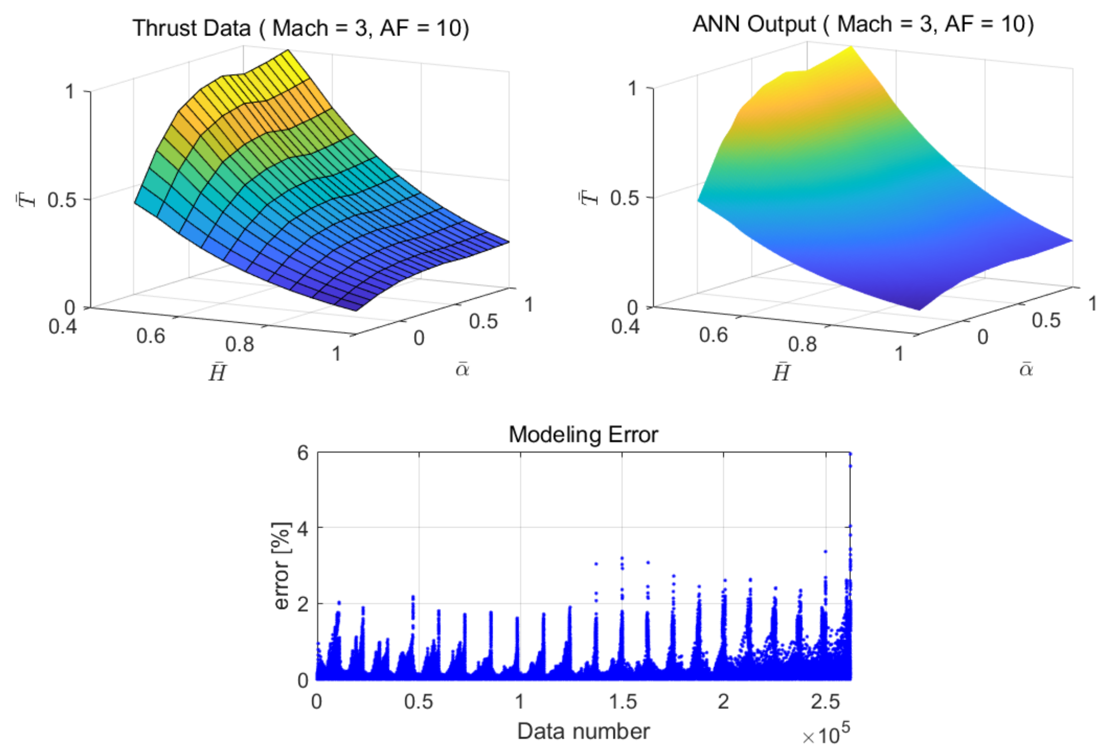

Figure 2: ANN training results for the thrust data sets

DOI: 10.13009/EUCASS2023-524

2.3 Minimum-final time problem

To define a trajectory optimization problem, proper boundary conditions should be set according to the purpose of the mission. The mid-course flight phase aims to reach the predicted intercept point (PIP) against the target. Initial boundary conditions are determined by the state of the missile at the beginning time $(t = t_0)$ of the mid-course phase.

$$x(t_0) = x_0,\ h(t_0) = h_0,\ V(t_0) = V_0,\ \gamma(t_0) = \gamma_0,\ m(t_0) = m_0 \tag{11}$$

Denoting the location for PIP to (x_f, h_f) and the dry mass for the missiles to m_b, terminal boundary conditions are written as follows.

$$x(t_f) = x_f,\ h(t_f) = h_f,\ m(t_f) \geq m_b \tag{12}$$

where t_f represents the final time, which is also an optimization variable to be minimized in this study. The minimum-final time problem for the VFDR missile can be written as follows.

$$\begin{aligned} &\text{minimize} && J = t_f \\ &\text{subject to} && \text{Eqs. (1)} - \text{(12)} \end{aligned} \tag{13}$$

3. Pseudospectral Sequential Convex Programming

3.1 System equation

This subsection defines the system equation for trajectory optimization. Based on Eq. (1), state and control variables are defined as follows.

$$\begin{aligned} \boldsymbol{z} &= [x,\ h,\ V,\ \gamma,\ m]^T \\ \boldsymbol{u} &= [\alpha,\ AF]^T \end{aligned} \tag{14}$$

Even though the angle-of-attack and fuel mass flow rate is utilized for controlling VFDR missiles, we select the air-to-fuel ratio instead of the fuel mass flow rate due to the previously mentioned advantages. The fuel mass flow rate can be inversely calculated from the optimization results using Eq. (5) and Eq. (9). Based on the defined state and control variables, the system equation can be written as follows.

$$\begin{aligned} &\boldsymbol{z} = \boldsymbol{f}(\boldsymbol{z}, \boldsymbol{u}) \\ &\text{where} \quad \boldsymbol{f}(\boldsymbol{z}, \boldsymbol{u}) = \begin{bmatrix} V\cos\gamma \\ V\sin\gamma \\ \dfrac{T\cos\alpha - D}{m} - g\sin\gamma \\ \dfrac{T\sin\alpha + L}{mV} - \dfrac{g\cos\gamma}{V} \\ -\dot{m}_f \end{bmatrix} \end{aligned} \tag{15}$$

In Eq. (15), this study utilizes Eq. (5) and Eq. (10) to calculate the fuel mass flow rate and thrust for trajectory optimization.

DOI: 10.13009/EUCASS2023-524

3.1 Pseudospectral discretization

In this subsection, the optimization problem in Eq. (13), defined in the continuous-time domain, is converted into the parameter optimization problem using the Legendre-Gauss-Radau (LGR) pseudospectral method [24]. The first step is to normalize the time domain from $t \in [t_0, t_f]$ to $\tau \in [-1, 1]$. Then, the system equation in Eq. (15) is altered as follows.

$$\frac{dz}{d\tau} = \begin{bmatrix} \frac{dx}{d\tau} & \frac{dh}{d\tau} & \frac{dV}{d\tau} & \frac{d\gamma}{d\tau} & \frac{dm}{d\tau} \end{bmatrix}^T = \frac{\eta}{2} \boldsymbol{f}(\boldsymbol{z}, \boldsymbol{u}) \tag{16}$$

where $\eta = t_f - t_0$ corresponds to the time normalization factor. We define the discretized state and control variables in the normalized time domain based on Eq. (14).

$$\begin{aligned} \boldsymbol{Z} &= \left[Z_1, Z_2, \cdots, Z_{N+1}\right]^T \quad \text{where } Z_i = \left[x_i, h_i, V_i, \gamma_i, m_i\right]^T \\ \boldsymbol{U} &= \left[U_1, U_2, \cdots, U_N\right]^T \quad \text{where } U_i = \left[\alpha_i, AF_i\right]^T \end{aligned} \tag{17}$$

where N represents the number of the collocation points, and $(\cdot)_i$ means $(\cdot)(\tau_i)$. Here, τ_i denotes the location of the discretized node, which is determined by the LGR pseudospectral method. Then, the system equation described in the continuous-time domain in Eq. (16) can be replaced by the following parametric equations.

$$\boldsymbol{DZ} = \frac{\eta}{2} \boldsymbol{F}(\boldsymbol{Z}, \boldsymbol{U}) \quad \text{where } \boldsymbol{F}(\boldsymbol{Z}, \boldsymbol{U}) = \left[\boldsymbol{f}(Z_1, U_1), \cdots, \boldsymbol{f}(Z_N, U_N)\right]^T \tag{18}$$

where $\boldsymbol{D}$ denotes the Radau differentiation matrix, in which each component is constant. The flight constraints in Eqs. (6)-(8) can be parametrized by the discretized state and control variables as follows.

$$\alpha_{\min} \le \alpha_i \le \alpha_{\max} \tag{19}$$

$$AF_{\min} \le AF_i \le AF_{\max} \tag{20}$$

$$\dot{m}_{f,\min} \le \dot{m}_f\left(V_i, h_i, \alpha_i, AF_i\right) \le \dot{m}_{f,\max} \tag{21}$$

for $i = 1, \cdots, N$. In Eq. (21), $\dot{m}_f(V_i, h_i, \alpha_i, AF_i)$ can be calculated by using Eq. (5) and Eq. (9). The boundary conditions in Eqs. (11)-(12) can be represented as follows.

$$Z_0 = \left[x_0, h_0, V_0, \gamma_0, m_0\right]^T \tag{22}$$

$$x_{N+1} = x_f, \; h_{N+1} = h_f, \; m_{N+1} \ge m_b \tag{23}$$

The performance index can also be replaced by using the time normalization factor (η). Then, the discretized minimum-final time problem can be written as follows.

$$\begin{aligned} &\text{minimize} && J = \eta \\ &\text{subject to} && \text{Eqs. } (18)-(23) \end{aligned} \tag{24}$$

DOI: 10.13009/EUCASS2023-524

3.3 Sequential convex programming

The discretized minimum-final time problem in Eq. (24) contains non-convex constraints in Eq. (18) and Eq. (21). This study applies the successive linearization method to solve the problem in the convex optimization framework. To this end, let us denote the previous k-th iterative solution for state and control variables to $Z_i^{(k)}$ and $U_i^{(k)}$. Then, the linearized system equation for the $(k+1)$-th iteration can be represented as follows.

$$\boldsymbol{D}_{r,i}\,\boldsymbol{Z}_r = \frac{\eta^{(k)}}{2}\boldsymbol{A}\left(Z_i^{(k)},\, U_i^{(k)}\right)Z_i + \frac{\eta^{(k)}}{2}\boldsymbol{B}\left(Z_i^{(k)},\, U_i^{(k)}\right)U_i + \frac{\boldsymbol{f}\left(Z_i^{(k)},\, U_i^{(k)}\right)}{2}\eta + \boldsymbol{R}^{(k)} \tag{25}$$

for $i = 1,\cdots,N$. Here, $\boldsymbol{D}_{r,i}$ and $\boldsymbol{Z}_r$ result from rearranging the Radau differentiation matrix $\boldsymbol{D}$ and discretized state variables $\boldsymbol{Z}$. The left side of Eq. (25) approximates the differentiation of the state variable in the normalized time domain, $dz/d\tau$ in Eq. (16), by a linear combination of the discretized state variables. The right side of Eq. (25) corresponds to the linearized equations for the right side of Eq. (16).

$$\begin{aligned} \boldsymbol{A}\left(Z_i^{(k)},\, U_i^{(k)}\right) &= \left.\frac{\partial \boldsymbol{f}}{\partial \boldsymbol{z}}\right|_{\left(Z_i^{(k)},\, U_i^{(k)}\right)}, \quad \boldsymbol{B}\left(Z_i^{(k)},\, U_i^{(k)}\right) = \left.\frac{\partial \boldsymbol{f}}{\partial \boldsymbol{u}}\right|_{\left(Z_i^{(k)},\, U_i^{(k)}\right)} \\ \boldsymbol{R}^{(k)} &= -\frac{\eta^{(k)}}{2}\left[\boldsymbol{A}\left(Z_i^{(k)},\, U_i^{(k)}\right)Z_i^{(k)} + \boldsymbol{B}\left(Z_i^{(k)},\, U_i^{(k)}\right)U_i^{(k)}\right] \end{aligned} \tag{26}$$

Next, we need to consider the restriction for the fuel mass flow rate in Eq. (21). Instead of applying successive linearization, this study replaces it with an equivalent linear constraint based on the basic concept of the pseudospectral method, which approximates the derivative of the state variables at each node as a linear combination of the discretized state variables, as in the left side of Eq. (25). Noting $\dot{m} = -\dot{m}_f$ and Eq. (16), the nonlinear constraint in Eq. (21) can be converted into the following equation.

$$-\frac{\eta}{2}\dot{m}_{f,\max} \le \left[\boldsymbol{D}_{r,i}\boldsymbol{Z}_r\right]_{(5,1)} \le -\frac{\eta}{2}\dot{m}_{f,\min} \tag{27}$$

where $[\boldsymbol{D}_{r,i}\boldsymbol{Z}_r]_{(5,1)}$ denotes the fifth row element of $\boldsymbol{D}_{r,i}\boldsymbol{Z}_r$. Note that Eq. (27) is an affine constraint with respect to the normalization factor and discretized state variables. By replacing the constraints in Eq. (18) and Eq. (21) with Eqs. (25)-(27), the discretized problem is modified to a convex optimization problem.

In applying SCP with successive linearization, trust-region constraints are considered to make the iterative solution not far away from the previous solution to validate the linear approximation. This study employes the following quadratic variable trust-region constraints [25].

$$\left(\left[(Z_i)^T,\,(U_i)^T\right] - \left[\left(Z_i^{(k)}\right)^T,\,\left(U_i^{(k)}\right)^T\right]\right)\left(\left[(Z_i)^T,\,(U_i)^T\right] - \left[\left(Z_i^{(k)}\right)^T,\,\left(U_i^{(k)}\right)^T\right]\right)^T \le s_i \tag{28}$$

for $i = 1,\cdots,N$. Here, s_i represents the variation of the state and control variable at each node, which also belongs to an optimization variable. Defining $\boldsymbol{s} = [s_1,\,\cdots,\,s_N]$, the total amount of variation is augmented to the performance index as a penalty term with a weighting value.

$$\hat{J}^{(k+1)} = \eta + \omega^{(k+1)}\left\|\boldsymbol{s}\right\|_2 \tag{29}$$

DOI: 10.13009/EUCASS2023-524

where $\omega^{(k+1)}$ corresponds to the weighting value for the $(k+1)$-th convex iteration. In this study, the weighting value is updated with the solution at each iteration according to the appropriateness of the solution process following the improved trust-region algorithm developed in [20]. Including the trust-region constraints and replacing the performance index, the convex sub-problem can be comprised as follows.

$$\begin{aligned} &\text{minimize} && \hat{J}^{(k+1)} = \eta + \omega^{(k+1)} \|\mathbf{s}\|_2 \\ &\text{subject to} && \text{Eqs. (19)} - \text{(20), (22)} - \text{(23), (25)} - \text{(28)} \end{aligned} \tag{30}$$

The solution for the original non-convex problem in Eq. (24) can be obtained by iteratively solving the convex sub-problem defined in Eq. (30) until the iterative solution converges within the prespecified tolerance.

$$\max_i \left(\left[\left(Z_i^{(k+1)}\right)^T, \left(U_i^{(k+1)}\right)^T \right] - \left[\left(\hat{Z}_i^{(k)}\right)^T, \left(\hat{U}_i^{(k)}\right)^T \right] \right) \le \varepsilon_{\text{tol}} \tag{31}$$

where $(\hat{\cdot})$ represents the solution after being updated by the improved trust-region algorithm.

Noting that SCP utilizes the previous iterative solution to compose the convex sub-problem, as revealed in Eq. (25), the initialization process is required for the first iteration. This study conducts a simple initialization process for state and control variables as follows.

$$\begin{aligned} x_i^{(0)} &= x_0 + \frac{\tau_i + 1}{2}\left(x_f - x_0\right) \\ h_i^{(0)} &= h_0 + \frac{\tau_i + 1}{2}\left(h_f - h_0\right) \\ V_i^{(0)} &= V_0 + \frac{\tau_i + 1}{2}\left(V_{up} - V_0\right) \\ \gamma_i^{(0)} &= \gamma_0 \\ m_i^{(0)} &= m_0 + \frac{\tau_i + 1}{2}\left(m_b - m_0\right) \\ \alpha_i^{(0)} &= \alpha_0 \\ AF_i^{(0)} &= AF_{\min} + \frac{\tau_i + 1}{2}\left(AF_{\max} - AF_{\min}\right) \\ \eta^{(0)} &= \frac{\sqrt{\left(x_f - x_0\right)^2 + \left(h_f - h_0\right)^2}}{0.5\left(V_0 + V_h\right)} \end{aligned} \tag{32}$$

where V_{up} is a design parameter to be selected as the expected final velocity. We select Mach number 4 at sea level for V_{up}. A linear interpolation is performed for the variables constrained on both sides (x, h, m). The variables constrained on one side and unpredictable (γ, α) are just set to their initial values. The variables that have increasing patterns (V, AF) during the flight are set to be linearly increased. The time normalization factor η is initialized as a division of the straight distance to the PIP by the expected average velocity.

4. Numerical Optimization Results

This section provides the trajectory optimization results for a VFDR missile obtained using the proposed algorithm. The first subsection shows the convergence pattern of the proposed algorithm, and the second subsection analyses the optimal trajectory pattern for the VFDR missile. MATLAB with MOSEK [26] was utilized for the implementation.

DOI: 10.13009/EUCASS2023-524

4.1 Convergence pattern

For a representative medium-range interception scenario, the convergence patterns for the proposed algorithm are depicted in Fig. 3. The proposed algorithm takes 21 iterations to converge the solution, and each iteration takes around 0.06 ~ 0.08 sec. Figure 3(a) shows that the engagement trajectory converges as the iteration progresses. Figure 3(b) represents both the original performance index in Eq. (13) and the augmented performance index in Eq. (30). They differ at early iterations but converge as the amount of the state and control variation decreases along the iterations, as depicted in Fig. 3(c). Figure 3(d) shows the weighting value for the penalty term at each iteration, which is automatically scheduled according to the validity of the solution process based on the improved trust-region algorithm.

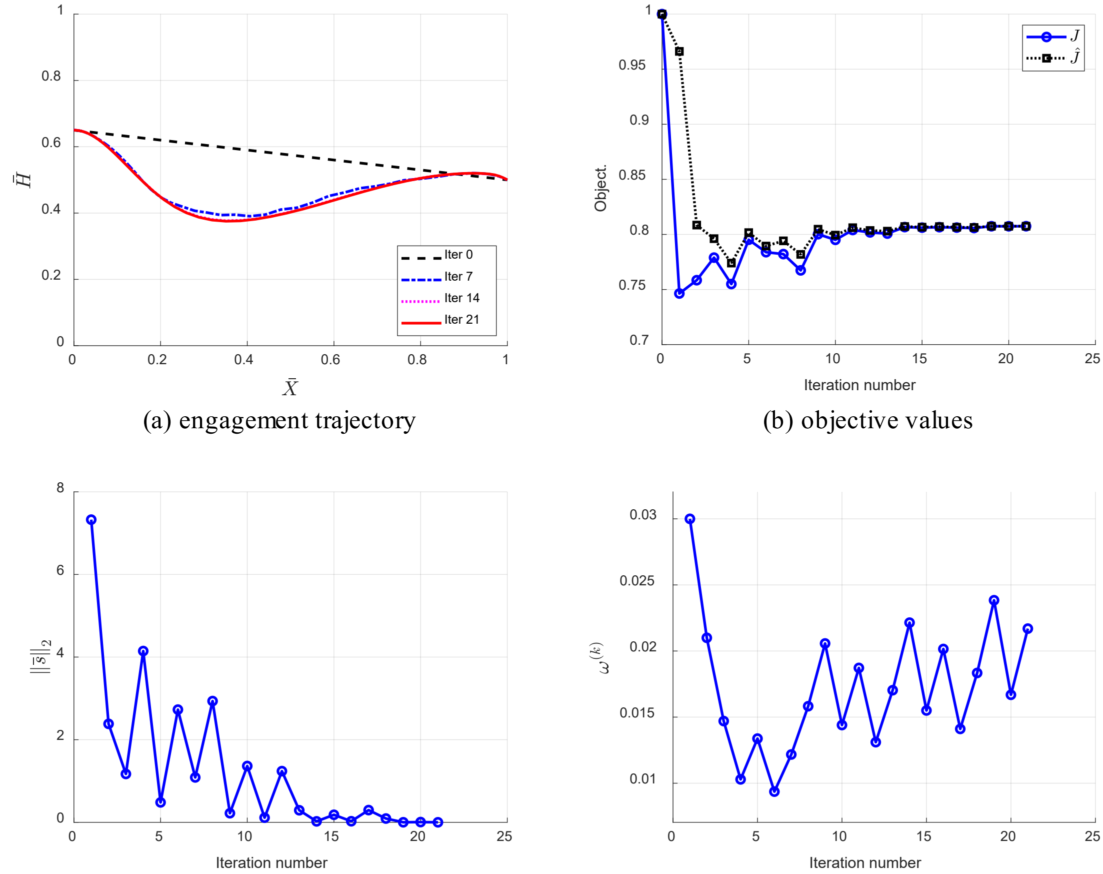

(a) engagement trajectory (b) objective values

(c) penalty term (d) weighting value

Figure 3: Convergence pattern analysis for the proposed algorithm: (a) engagement trajectory, (b) objective values, (c) penalty term, and (d) weighting value

4.2 Optimal trajectory patterns

This subsection compares the optimization results for two different engagement scenarios: the medium-range engagement, presented in the previous section, and the long-range engagement. The comparison results are depicted in Fig. 4. One notable observation is that the missiles commonly descend at the initial time, as shown in Fig. 4(a) and Fig. 4(b), in contrast to the solid rocket missiles ascending to reduce the drag by reaching the low-air density area. It comes from the fact that the specific impulse of the VFDR engine depends on the flight conditions, such as Mach number, altitude, angle-of-attack, and air-to-fuel ratio. One feature of the VFDR engine is that the specific impulse increases as the air-to-fuel ratio increases [21]. Hence, it can be interpreted as the missiles initially descend to absorb more air mass flow rate by increasing the velocity and reaching high-air density area. It results in increasing the air-to-fuel ratio as depicted in Fig. 4(d) for both engagement scenarios. However, in contrast to the medium-range scenario, it can be seen that the missile in the long-range scenario climbs up after the first descending. This pattern seems to

DOI: 10.13009/EUCASS2023-524

reduce the drag, as for solid rocket missiles, after ensuring sufficient air mass flow rate by accelerating the missile enough.

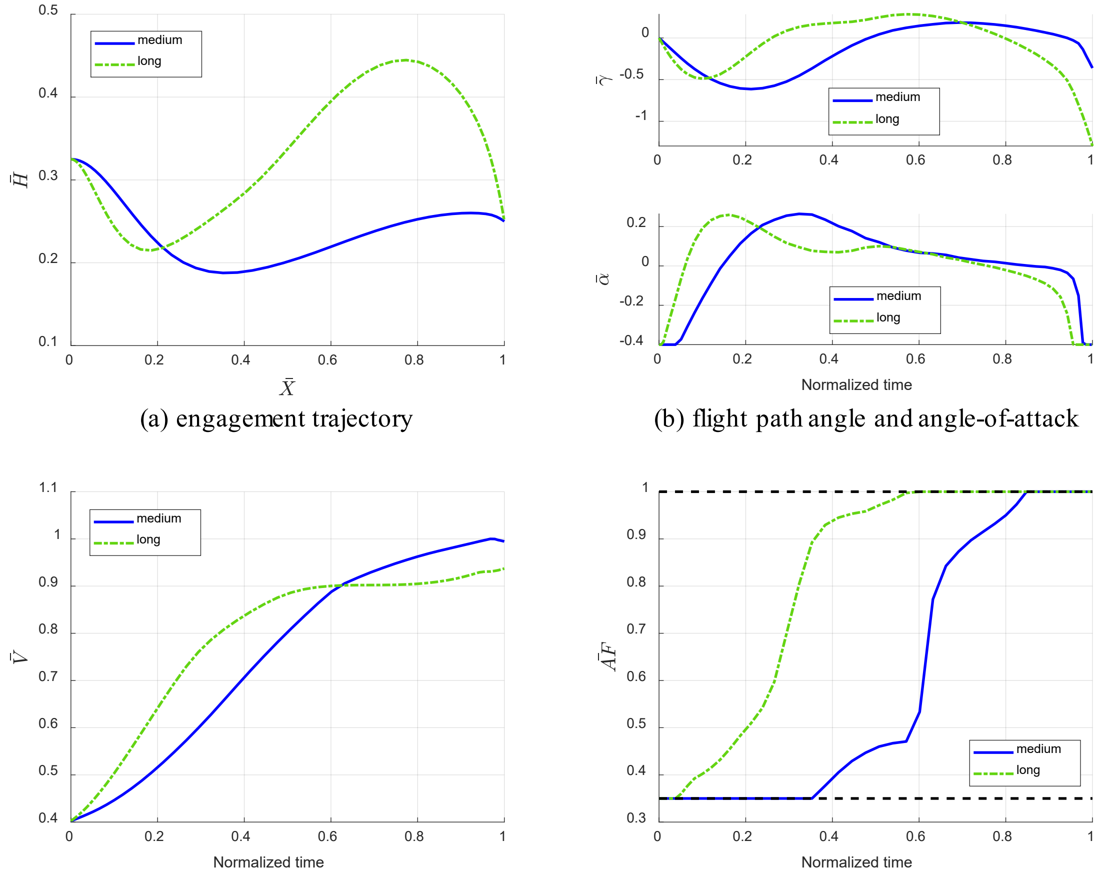

(a) engagement trajectory

(b) flight path angle and angle-of-attack

(c) velocity

(d) air-to-fuel ratio

Figure 4: Optimal trajectory pattern analysis for the proposed algorithm: (a) engagement trajectory, (b) flight path angle and angle-of-attack, (c) velocity, and (d) air-to-fuel ratio

5. Conclusions

This paper developed a mid-course trajectory optimization algorithm for VFDR missiles based on convex optimization. The angle-of-attack influence function was obtained for the air mass flow rate, and the ANN was constructed by training the thrust data. The air-to-fuel ratio was selected as a control variable to establish the system equation. The LGR pseudopsectral method was applied to discretize the problem. The fuel mass flow rate limit, which corresponds to a nonlinear constraint, was altered to an equivalent affine constraint. Then, a convex sub-problem was composed by incorporating variable trust-region constraints and solved using a commercial solver with an improved trust-region algorithm. The proposed algorithm took around 1.5 ~ 2.0 sec to solve the problems, and the convergence patterns were presented. The optimization results revealed that the VFDR missiles have a distinct trajectory pattern from traditional solid rocket missiles according to the feature of the VFDR engine, whose specific impulse depends on the flight conditions.

Acknowledgements

This work was supported by the Theater Defense Research Center funded by Defense Acquisition Program Administration under Grand UD200043CD.

DOI: 10.13009/EUCASS2023-524

References

[1] Imado, F., Kuroda, T., and Miwa, S. (1990). Optimal midcourse guidance for medium-range air-to-air missiles. *Journal of Guidance, Control, and Dynamics, 13*(4). 603-608.

[2] Cheng, V. H. L. and Gupta, N. K. (1986). Advanced midcourse guidance for air-to-air missiles. *Journal of Guidance, Control, and Dynamics, 9*(2). 135-142.

[3] Cheng, V. H. L., Menon, P. K. A., Gupta, N. K., and Briggs, M. M. (1987). Reduced-order pulse-motor ignition control logic. *Journal of Guidance, Control, and Dynamics, 10*(4), 343-350.

[4] Menon, P. K. A. and Briggs, M. M. (1990). Near-optimal midcourse guidance for air-to-air missiles. *Journal of Guidance, Control, and Dynamics, 13*(4). 596-602.

[5] Manickavasagam, M., Sarkar, A. K., and Vaithriyanathan, V. (2017). A Singular Perturbation based Midcourse Guidance Law for Realistic Air-to-air Engagement. *Defence Science Journal, 67*(1).

[6] Annam, C., Ratnoo, A., and Ghose, D. (2021). Singular-perturbation-based guidance of pulse motor interceptors with look angle constratins. *Journal of Guidance, Control, and Dynamics, 44*(7), 1356-1370.

[7] Katzir, S., Cliff, E. M., and Lutze, F. H. (1989). An approach to near optimal guidance on-board calculations. In *Proceedings. ICCON IEEE International Conference on Control and Applications* (pp. 133-139). IEEE.

[8] Kumar, R. R., Seywald, H., and Cliff, E. M. (1995). Near-optimal three-dimensional air-to-air missile guidance against maneuvering target. *Journal of Guidance, Control, and Dynamics, 18*(3), 457-464.

[9] Yang, S. M. (1996). Analysis of optimal midcourse guidance law. *IEEE Transactions on Aerospace and Electronic Systems, 32*(1), 419-425.

[10] Goldstein, F. and Calise, A. (1983). Adaptive control of variable flow ductd rockets. In *Guidance and Control Conference* (p. 2202)

[11] Kuroda, T., Mihara, S., Matsuda, H., Hirokawa, R., and Imado, F. (1998). Optimal mid-course guidance of variable flow ducted rocket missiels. In *Guidance, Navigation, and Control Conference and Exhibit* (p. 4213)

[12] Halswijk, W. (2009). Online dynamic flight optimisation applied to guidance of a variable-flow ducted rocket. In *AIAA Guidance, Navigation, and Control Conference* (p. 6090).

[13] Fahroo, F. and Ross, I. M. (2002). Direct trajectory optimization by a Chevyshev pseudospectral method. *Journal of Guidance, Control, and Dynamics, 25*(1), 160-166.

[14] Szmuk, M., Acikmese, B., and Verning, A. W. (2016). Successive convexification for fuel-optimal powered landing with aerodynamic drag and non-convex constraints. In *AIAA Guidance, Navigation, and Control Conference* (p. 0378).

[15] Liu, X., Shen, Z., and Lu, P. (2016). Exact convex relaxation for optimal flight of aerodynamically controlled missiles. *IEEE Transactions on Aerospace and Electrnoic System, 52*(4), 1881-1892.

[16] Liu, X., Shen, Z., and Lu, P. (2016). Entry trajectory optimization by second-order cone programming. *Journal of Guidance, Control, and Dynamics, 39*(2), 227-241.

[17] Wang, J. and Cui, N. (2018). A pseudospectral-convex optimization algorithm for rocket landing guidance. In *2018 AIAA Guidance, Navigation, and Control Conference* (p. 1871).

[18] Sagliano, M. And Mooij, E. (2021). Optimal drag-energy entry guidance via pseudospectral convex optimization. *Aerospace Science and Technology, 117*, 106946.

[19] Wang, J., Cui, N., and Wei, C. (2019). Rapid trajectory optimization for hypersonic entry using convex optimization and pseudospectral method. *Aircraft Engineering and Aerospace Technology, 91*(4), 669-679.

[20] Kim, B. and Lee, C. H. (2023). Optimal midcourse guidance for dual-pulse rocket using pseudospectral sequential convex programming. *Journal of Guidance, Control, and Dynamics, 46*(7), 1425-1436.

[21] Lee, Y. And Sung, H. G. (2023). Performance modeling of a ducted rocket. *Journal of Korean Society for Aeronautical and Space Sciences, 51*(1), 9-17.

[22] Herrmann, D. And Gülhan, A. (2010). Influence of intake orientation on ramjet performance. *Journal of Propulsion and Power, 26*(4), 848-857.

[23] Hornik, K., Stinchcombe, M., and White, H. (1989). Multilayer feedforward networks are universal approximators. *Neural networks*, 2(5), 359-366.

[24] Garg, D., Patterson, M., Hager, W. W., Rao, A. V., Benson, D. A., and Huntington, G. T. (2010). A unified framework for the numerical solution of optimal control problems using pseudospectral methods. *Automatica, 46*(11), 1843-1851.

[25] Wang, Z. and Lu, Y. (2020). Improved sequential convex programming algorithms for entry trajectory optimization. *Journal of Spacecraft and Rocekts, 57*(6), 1373-1386.

[26] ApS, M. (2019). Mosek optimization toolbox for matlab. *User's Guide and Reference Manual, Version, 4,* 1.